Antiferromagnet-controlled spin current transport in $SrMnO_3$/Pt hybrids

J. H. Han,[1] C. Song,[1,*] F. Li,[1] Y. Y. Wang,[1] G. Y. Wang,[1] Q. H. Yang,[2] and F. Pan[1]

[1]*Key Laboratory of Advanced Materials (MOE), School of Materials Science and Engineering, Tsinghua University, Beijing 100084, China*

[2]*State Key Laboratory of Electronic Films and Integrated Devices, University of Electronic Science and Technology of China, Chengdu 610054, China*

(Received 26 August 2014; revised manuscript received 7 October 2014; published 27 October 2014)

We investigate the spin Hall magnetoresistance (SMR) in $SrMnO_3$ (SMO)/Pt hybrids, where SMO is an antiferromagnetic (AFM) insulator. The AFM moments partially rotate with out-of-plane magnetic fields, producing room-temperature SMR. By manipulating the electron spins in Pt, we observe Larmor precession-induced oscillating SMR, reaffirming the spin current transport determined by the relative arrangement between the Pt electron spins and AFM moments. The use of the AFM with no net moments annihilates the magnetic proximity effect and thus confirms the SMR origination from AFM-controlled spin current transport, with significant spin mixing conductance of $\sim 10^{17}$ m^{-2}. Our findings provide an interesting perspective to detecting AFM moments and represent a significant step towards AFM spintroincs.

DOI: 10.1103/PhysRevB.90.144431 PACS number(s): 75.50.Ee, 75.70.−i, 85.75.Nn

I. INTRODUCTION

The ferromagnet/nonmagnetic metal (FM/NM) hybrid structures stand out as a seminal model in the emerging field of spintronics, producing a rich spectrum of exotic properties including spin valve effect, spin injection, and spin pumping [1–4], etc. As a paramagnetic metal with large spin-orbit coupling, Pt plays a fundamental role in the conversion between charge current and spin current based on the spin Hall effect and the inverse spin Hall effect, establishing most of the recent spin-related phenomena in FM/Pt bilayers [5,6]. The spin Hall magnetoresistance (SMR) and the spin Seebeck effect are two interesting observations when Pt is attached to a ferromagnetic insulator $Y_3Fe_5O_{12}$ (YIG), both of which are related to a pure spin current flowing along the direction normal to the YIG/Pt interface [5–9]. Unfortunately, the possible existence of the magnetic proximity effect (MPE) at the YIG/Pt interface complicates the detection of the SMR signals [10–16]. Similarly, the MPE-induced FM ordering in the Pt film associated with the anomalous Nernst effect becomes an obstacle for the quantitative characterizations of the spin Seebeck effect, due to an induced spin polarized current parallel with the spin current [16–19]. Several methods have been employed to confirm the spin-relevant behavior and to exclude the MPE, e.g., the introduction of a copper insert between YIG and Pt [5], replacement of Pt by the element far from the Stoner instability (Au or Ta) [20,21], and interface modification [16].

The existence of ferromagnetic stray fields and the sensitivity of FM moments to magnetic field perturbations in FM/NM structures pose great obstacles for high-density memory integration. To eliminate these unfavorable factors, applications of antiferromagnets (AFMs) in spintronics [22,23] are attracting increasing interest much beyond their current passive role in exchange bias. The absence of stray fields and the rigidity to external magnetic fields make AFM particularly favorable for the mutual control of the spin transport and magnetic properties [24], leading to ultrafast and ultrahigh-density spintronics. Besides AFM-based magnetic tunnel junctions in which tunneling anisotropic magnetoresistance has been obtained recently [25,26], as-yet-unexplored AFM/Pt hybrids are especially favored for the direct study on the interactions between AFM moments and spin current. Due to the absence of net moments in AFM, it provides an intrinsic advantage over its FM counterpart for excluding the MPE. However, the question comes naturally about how to manipulate the AFM moments at the AFM/Pt interface. More challenging is the difficulty of unraveling the AFM moments through the magnetotransport signals. The experiments described below create changeable relative spin arrangement between antiferromagnetic $SrMnO_3$ (SMO) and Pt, giving rise to unprecedented spin current transport in AFM/Pt hybrids, which is manifested by the SMR of the Pt layer.

II. EXPERIMENTAL METHODS

The highly insulating single-crystalline (001) SMO film with the thickness of 8 nm was grown on an insulating (001) $SrTiO_3$ substrate by pulsed laser deposition, followed by an ultrathin Pt film (3 or 7 nm) deposited by magnetron sputtering. SMO is a typical *G*-type AFM, whose moments in the (001) plane are aligned completely antiparallel with compensated spins, exhibiting no net ferromagnetism [Fig. 1(a)]. Consequently, the possible MPE at the SMO/Pt interface is naturally excluded, eradicating the contamination of the spin current in Pt. We use four-probe measurements on patterned Pt Hall-bar thin films. A schematic of the sample layout is shown in Fig. 1(b), where the film plane is in the *xy* plane with a constant channel current $\boldsymbol{I}$ of 100 μA along the *x* direction, while the longitudinal resistance is measured by the two side electrodes with the distance of 400 μm.

III. RESULTS AND DISCUSSION

A. Observation of the SMR in AFM/Pt hybrids

We first show in Fig. 2(a) the longitudinal resistance R_{xx} of the 7-nm-thick Pt sample as a function of out-of-plane magnetic fields ($\boldsymbol{H}$) at room temperature. The most striking result here is the observation of a positive magnetoresistance,

*Corresponding author: songcheng@mail.tsinghua.edu.cn

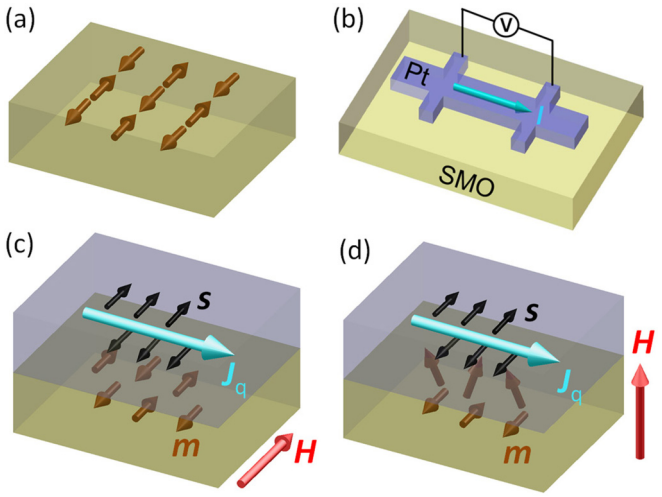

FIG. 1. (Color online) (a) The AFM moment arrangement in the (001) plane of SMO. (b) A schematic of the sample layout. (c) Low resistance state at the zero field or with in-plane H. (d) High-resistance state with out-of-plane H. The SMR is determined by the interfacial relative arrangement between the electron spins ($\boldsymbol{s}$) in Pt and the AFM moments ($\boldsymbol{m}$) in SMO.

where R_{xx} reaches its minimum around the zero field and increases with the external field. The magnitude of the varied R_{xx} is calculated to be ~0.035 Ω with respect to the resistance difference at 9 T and the zero field, corresponding to the magnetoresistance ratio of 10^{-2}%. This value is comparable to (10^{-2}% for [5]) or even larger than (10^{-3}% for [27]) that at the Pt/YIG interface. The magnetoresistance obtained in thinner Pt samples (3 nm), as presented in Fig. 2(b), shows the same qualitative behavior, but with an enhanced overall magnitude of ~0.25 Ω.

We now focus on the correlation between the magnetoresistance and the spin arrangement in SMO with field sweeping. When a charge current is applied to the Pt layer, the flow of electrons with opposite spin directions in the Pt layer

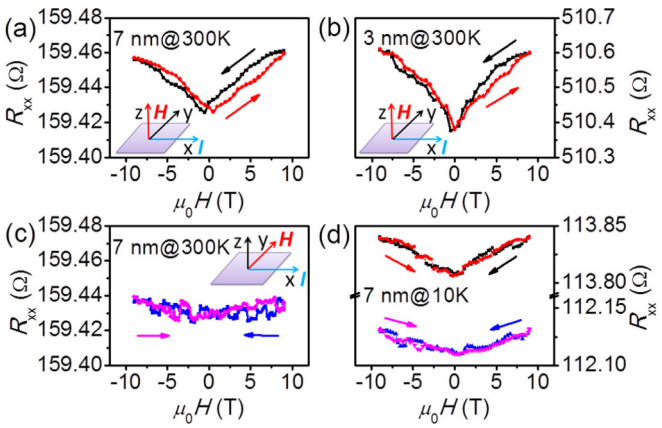

FIG. 2. (Color online) (a) and (b) Resistance curves of SMO/Pt (7 nm) and SMO/Pt (3 nm) when sweeping an out-of-plane H at room temperature. (c) Resistance curve of SMO/Pt (7 nm) when sweeping an in-plane H at room temperature. (d) Resistance curves of SMO/Pt (7 nm) when sweeping out-of-plane and in-plane H at 10 K after out-of-plane and in-plane field-cooling treatments, respectively.

deflects upwards and downwards, driven by the spin Hall effect. The resultant spin current density $\boldsymbol{J}_s \propto \alpha_{SH} \boldsymbol{J}_q \times \boldsymbol{s}$($\alpha_{SH}$ are parameters of the spin Hall angle) is in the direction perpendicular to the charge current density $\boldsymbol{J}_q$ and the spin direction $\boldsymbol{s}$. Rationally, the electron spins $\boldsymbol{s}$ in Pt arriving at the interface have a component parallel to the AFM moments ($\boldsymbol{m}$) in SMO in the vicinity of the interface, resulting in minimum spin Hall torque absorption and maximum reflection into the Pt layer itself. It is then transformed to an additional charge current parallel to the original one through the inverse spin Hall effect ($\boldsymbol{J}_q^{add} \propto \alpha_{SH} \boldsymbol{J}_s \times \boldsymbol{s}$) and results in the minimum resistance around the zero field [Fig. 1(c)] [2,6]. Once the equilibrium of the upward and downward deflecting is established, a pure spin current is injected across the SMO/Pt interface. The AFM moments in the SMO layer partially rotate with out-of-plane $\boldsymbol{H}$, and tend to be perpendicular to the electron spins deflecting from the Pt layer, which results in large absorption and small reflection associated with a slight increase of the channel resistance [Fig. 1(d)]. Differently, the SMR vanishes when the Pt film is deposited on nonmagnetic SiO_2 substrates, since no spin current passes the SiO_2/Pt interface. Such spin current transport is supported by the previous work that spin transfer torques were realized in AFM-based magnetic tunneling junctions [4,22,26].

Although the electrons do not enter into the electrically insulating SMO, the resistance of the Pt film reflects the AFM-controlled relative arrangement between the electron spins in Pt and the AFM moments in SMO. The magnetoresistance is referred to as the well-known SMR, taking its association with the spin current into account [5]. A closer inspection of the resistance curves in Figs. 2(a) and 2(b) shows that a hysteresis exists when $\boldsymbol{H}$ is swept up and ramped down, which is most likely ascribed to the hysteretic characteristics of the AFM moments. Apparently, the SMR in AFM/Pt systems is free from the possible MPE which probably complicates the detection of the SMR and the spin Seebeck effect in YIG/Pt, thus unambiguously confirming the magnetoresistance from the spin current transport at the magnet/Pt interface.

Generally, the magnitude of the observed SMR is correlated to the spin mixing conductance at the SMO/Pt interface. The transformation between the charge current flowing through the Pt layer and the spin current dominated by the SMO/Pt interface can be theoretically performed as [28–30]

$$J_s = \frac{g_{\uparrow\downarrow}}{2\pi} 2e\lambda_{SD}\rho_{Pt}\alpha_{SH} J_q \tanh\frac{t_{Pt}}{2\lambda_{SD}}\eta, \tag{1}$$

in which we introduce the correction factor

$$\eta = \left(1 + 2g_{\uparrow\downarrow}\rho_{Pt}\lambda_{SD}\frac{e^2}{h}\coth\frac{t_{Pt}}{\lambda_{SD}}\right)^{-1}. \tag{2}$$

The spin current density can be extracted from the SMR data as

$$J_s = J_q \frac{\Delta\rho}{\rho_0}\frac{\hbar t_{Pt}}{\alpha_{SH} e\lambda_{SD}\tanh\frac{t_{Pt}}{2\lambda_{SD}}}, \tag{3}$$

where $g_{\uparrow\downarrow}$ is the spin mixing conductance per unit of interface area and the conductance quantum e^2/h, e is the electronic charge, h is the Planck constant, the spin diffusion length of Pt is $\lambda_{SD} = 1.5$ nm, the Pt resistivity is $\rho_{Pt} = 2.22 \times 10^{-7}$ Ω m,

$\alpha_{SH} = 0.11$ is the spin Hall angle of Pt, $\Delta\rho$ is the SMR-related resistivity change, and ρ_0 represents the ordinary Pt resistivity as a constant resistivity offset, which is equal to ρ_{Pt} as a calculating approximation [28–30]. Taken together, the relationship between $\Delta\rho$ and $g_{\uparrow\downarrow}$ can be expressed by

$$\frac{\Delta\rho}{\rho_{Pt}} = \left(\frac{2e^2\lambda_{SD}^2\rho_{Pt}\alpha_{SH}^2}{ht_{Pt}}\tanh\frac{t_{Pt}}{2\lambda_{SD}}\right) g_{\uparrow\downarrow}\tanh\frac{t_{Pt}}{2\lambda_{SD}}\eta. \quad (4)$$

For the case of SMO/Pt (7 nm), we estimate that the magnitude of the SMR is between 0.035 and 0.05 Ω, taking the tendency of the resistance curve in Fig. 2(a) into consideration though the SMR is still unsaturated with the external field up to 9 T. Consequently, the spin mixing conductance of the SMO/Pt interface is $3.4 \times 10^{17}\ \mathrm{m}^{-2} < g_{\uparrow\downarrow} < 4.9 \times 10^{17}\ \mathrm{m}^{-2}$, which is close to that of the YIG/Pt interface ($\sim 10^{18}\ \mathrm{m}^{-2}$) [31,32], indicating the significant spin-dependent conductance at the AFM/Pt interface and the feasibility of building a spin current detector via the AFM/metal interface. The comparable spin mixing conductance also substantiates the aforementioned equivalent magnetoresistance ratio between SMO/Pt and YIG/Pt systems.

The situation turns out to be dramatically different when the external $\boldsymbol{H}$ is applied in plane and perpendicular to the current $\boldsymbol{I}$. Figure 2(c) displays a nearly constant R_{xx} of the 7-nm sample with field sweeping, suggesting no magnetoresistance in this scenario. For in-plane field sweeping, the AFM moments in SMO are more stubborn to change their directions than the situation with out-of-plane sweeping, and are almost fixed along the initial directions even if a very large field up to 9 T is applied (the largest field of our transport measurement setup), as illustrated in Fig. 1(c). This observation is in analogy to the stable IrMn moments pinned along its easy direction [23,25]. Hence, the electron spins in Pt are persistently reflected at the SMO/Pt interface back to the Pt channel, leading to a large spin current injection and thus a consistently low resistance state. Interestingly, this claim is fully supported by the fact that R_{xx} in Fig. 2(c) is approaching minimum R_{xx} in Fig. 2(a), i.e., 159.43 Ω around the zero field, because both of these two states have a similar spin arrangement determined by the interfacial AFM moments [30].

Given that the AFM moments cannot be completely parallel to $\boldsymbol{H}$ at 300 K, just below the Néel temperature of SMO (~350 K) [33], we cool the 7-nm sample with an out-of-plane field of 9 T from 400 to 10 K. Meanwhile, a field-cooling procedure with an in-plane field is carried out for comparison. Corresponding magnetoresistance curves recorded at 10 K are shown in Fig. 2(d). For out-of-plane field cooling, the AFM moments $\boldsymbol{m}$ of SMO are almost arranged along the direction of $\boldsymbol{H}$, which is perpendicular to the electron spins $\boldsymbol{s}$ (in-plane), resulting in a minimum spin current injection. In contrast, the in-plane cooling field arranges the $\boldsymbol{m}//\boldsymbol{s}$ along the y axis, accompanied by a maximum injection. As a result, the out-of-plane R_{xx} is remarkably higher than its in-plane counterpart even at the zero field at 10 K [Fig. 2(d)], in contrast to the aforementioned scenario at 300 K without any field-cooling process. Meanwhile, the SMR with out-of-plane fields is clearly larger than that with in-plane fields, similar to the case at 300 K. The signal with in-plane fields shows subtle magnetoresistance, because the sample plane cannot be strictly parallel to the cooling field in the experiment. To sum up, the SMR enables direct electrical sensing of the moment rotation in the insulating antiferromagnetic SMO.

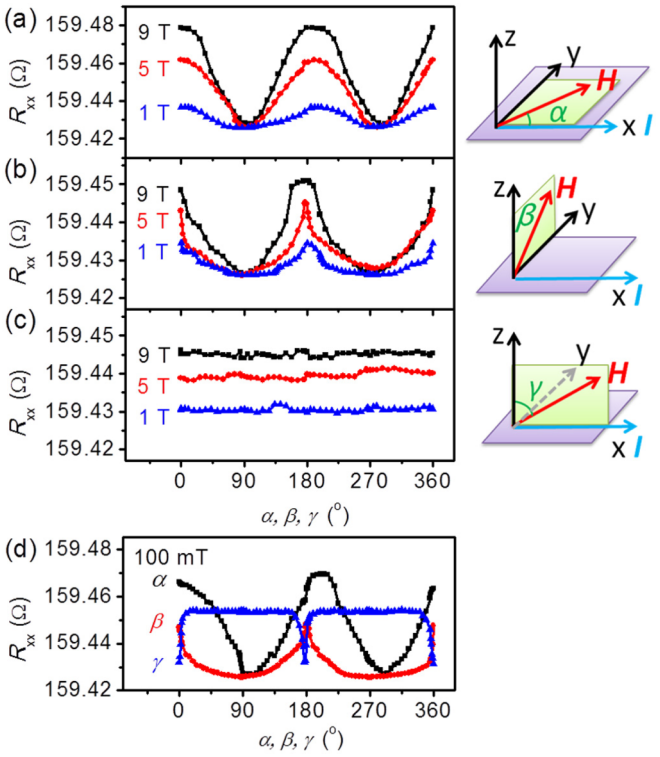

FIG. 3. (Color online) (a)–(c) α, β, and γ dependence of the resistance in SMO/Pt (7 nm), where α, β, and γ are defined in the schematics related to each resistance curve. The α, β, and γ curves are all measured under the H of 1, 5, and 9 T, respectively. (d) The dependence of the Pt resistance in YIG/Pt (7 nm) on α, β, and γ when rotating a magnetic field of 100 mT. All the data were recorded at 300 K.

B. Angular dependence of the SMR

We then turn towards the angular dependence of the SMR. For these angle-dependent resistance measurements, the resistance evolutions of the 7-nm sample as a function of representative magnetic fields (1, 5, and 9 T) applied in the xy plane (α scan), yz plane (β scan), and xz plane (γ scan) are presented in Figs. 3(a)–3(c), respectively. The SMR can be formulated as $\rho_{xx} = \rho_0 + \Delta\rho m_y^2$, where m_y are parameters of the normalized y component of the interfacial AFM moments. Consequently, the α scan and β scan curves at room temperature show the $\cos^2\alpha$ and $\cos^2\beta$ dependence with a period of 180°, respectively [Figs. 3(a) and 3(b)], giving rise to the maximum R_{xx} at 0° and 180°, in contrast to the minimum R_{xx} at 90° and 270° where $\boldsymbol{H}$ is parallel to $\boldsymbol{s}$. Given that the AFM moments do not rotate when the in-plane field is swept, associated with the absence of SMR [Fig. 2(c)], it is surprising to see the angle-dependent R_{xx} in Fig. 3(a) for various in-plane fields. This observation could be explained by the AFM moments in SMO being easier to rotate gradually when driven by a large rotating field than to reverse abruptly when sweeping the magnetic field, producing

a stronger spin absorption for $\boldsymbol{H}//\boldsymbol{I}$ compared with that for $\boldsymbol{H} \perp \boldsymbol{I}$, and thus a higher resistance for the former case (0° and 180°). Such moment rotation in the AFM insulator is supported by similar findings in AFM semiconductors and manganites [34,35].

A closer check of the β scan curves in Fig. 3(b) shows that the R_{xx} valleys at 90° and 270° are much wider than the R_{xx} peaks at 0° and 180°, reflecting that the SMO moments tend to align in plane rather than out of plane, which is an intrinsic feature for almost all the AFM materials. It is noteworthy that the magnitude of R_{xx} is enhanced with the increasing fields from 1 to 9 T, indicating that the AFM moments are prone to align along the high external fields. This is different from the case of YIG/Pt (7 nm), in which the angle-dependent R_{xx} is not sensitive to external fields and 100 mT is sufficient to orient the magnetization of YIG, as displayed in Fig. 3(d). In addition, according to the theory of the SMR, R_{xx} should not change with $\boldsymbol{H}$ when it is rotated in the xz plane (γ scan), because the relative spin arrangement at the interface is almost immutable, irrespective of the directions of $\boldsymbol{H}$ in this plane. This is echoed in the γ-dependent R_{xx} in Fig. 3(c), where it stays consistent except for some signal-to-noise fluctuations, even with H up to 9 T. Similarly, the angular dependence of R_{xx} vanishes for the γ scan for the YIG/Pt, but has sharp valleys at 0° and 180° due to the abrupt in-plane reorientation of the magnetization [Fig. 3(d)].

C. Oscillating SMR induced by the Larmor precession

The manipulation of the AFM moments has revealed that the SMR originates from the spin current transport at the SMO/Pt interface, which directly indicates the indispensable control by the AFM. Given that the SMR is determined by the relative configuration between the electron spins in Pt and the AFM moments in SMO at the interface, we now address the question whether the SMR can also be observed by tuning the electron spins in the Pt layer. The electron spins $\boldsymbol{s}$ undergo a Larmor precession when an out-of-plane magnetic field is swept from 0 to 50 mT with a small step of ~0.5 mT, which is essential to observe the detailed oscillations. Remarkably, strong oscillations of the SMR due to the Larmor precession are clearly observed in Fig. 4(a). At the zero field, $\boldsymbol{s}$ are parallel to the $\boldsymbol{m}$ component along the y axis accompanied by a large spin current injection, allowing the R_{xx} signal at its minimum value (point I). The magnetic field below 50 mT is too low to drive the rotation of the AFM moments, which keep the in-plane collinear arrangement unchangeably and provide a reference direction of the electron spins in Pt. Nevertheless, such a low magnetic field is large enough to drive the electron spins in Pt to undergo the Larmor precession, which is performed as $\frac{d\boldsymbol{s}}{dt} = \frac{e\mu_0}{2m_e}\boldsymbol{H} \times \boldsymbol{s}$. This precession leads to a gradual change of the relative arrangements between $\boldsymbol{s}$ and $\boldsymbol{m}$ with a periodicity of 180°, as illustrated in Fig. 4(b), where $\boldsymbol{s}$ are coplanar with $\boldsymbol{m}$ again, corresponding to the R_{xx} valley (point II). With further increasing field, oscillations remain. This process is somehow similar to the Hanle effect, referring to spin precession, which commonly serves as a criterion for spin injection [36]. Such oscillations disappear after cooling from 400 to 10 K with an out-of-plane field of 9 T (not shown),

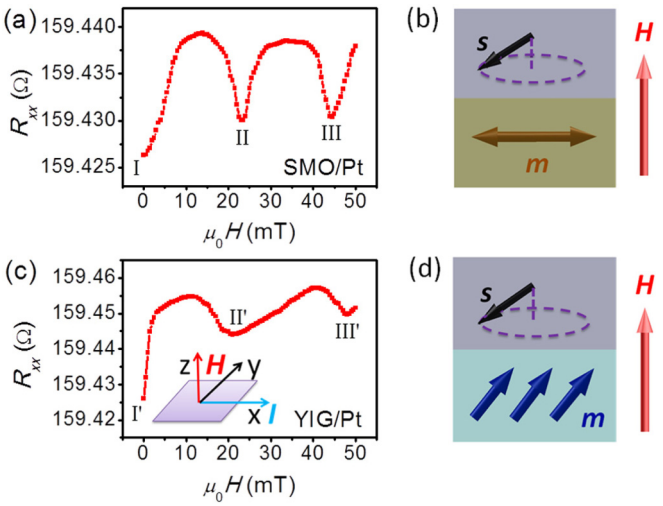

FIG. 4. (Color online) Oscillating resistance signals induced by the Larmor precession in the Pt layer for (a) SMO/Pt (7 nm) and (c) YIG/Pt (7 nm) bilayers when sweeping a small out-of-plane magnetic field at 300 K. The magnetic field starts from 0 to 50 mT in small steps (~0.5 mT). Corresponding schematics of the Larmor precession in SMO/Pt and YIG/Pt bilayers are shown in (b) and (d), respectively.

because the AFM moments in SMO are almost aligned out of plane, making the stable angle between $\boldsymbol{s}$ and $\boldsymbol{m}$ even if the Larmor precession occurs.

Figure 4(c) presents similar R_{xx} oscillations in the YIG/Pt (7 nm) sample, corroborating that the tuning of spin precession in Pt affects the spin current–dependent dynamics at the magnet/Pt interface, irrespective of AFM or FM. Nevertheless, the latter shows attenuated signals with increasing field by comparing point III′ with point II′, different from the more comparable magnitudes of the former between point III and point II. This behavior could be explained by the fields within 50 mT being able to cause spin precession in Pt and a slight moment rotation of magnetically soft YIG simultaneously [Fig. 4(d)], with the result that the angular variation of spins in YIG/Pt is not so remarkable as the case in SMO/Pt. Notably, the observed oscillatory behavior cannot be explained by the de Haas–van Alphen effect: (1) The data do not show the $1/B$ periodicity; (2) the present measurements were carried out at room temperature; (3) it cannot explain the oscillatory difference for the SMO/Pt and YIG/Pt samples. Consequently, the Larmor precession of the electron spins in Pt not only provides compelling evidence for the indirect AFM-controlled spin current transport for the SMR, but also adds an additional dimension to the detection of AFM moments with small magnetic fields.

IV. SUMMARY

In the present study we demonstrate that the observed SMR in the AFM/metal hybrids, manipulated by the interfacial relative arrangement between the electron spins in Pt and the AFM moments in SMO, originates from the AFM-controlled spin current transport. The SMO/Pt interface possesses a spin mixing conductance comparable to typical FM/Pt hybrids, reflecting the significance of the AFM/Pt interface for

spin-related phenomena. Our work presents a broad opportunity to investigate AFM/metal bilayers, which would provide a different viewpoint to clarify the rich spin-dependent effects at the FM/Pt interface observed very recently, and open another avenue for the development of AFM spintronics.

ACKNOWLEDGMENTS

This work was supported by the National Natural Science Foundation of China (Grants No. 51322101, No. 51202125, and No. 51231004) and National Hi-tech (R&D) project of China (Grants No. 2014AA032904 and No. 2014AA032901).

[1] J. Sinova and I. Žutić, Nat. Mater. **11**, 368 (2011).
[2] A. Brataas, A. D. Kent, and H. Ohno, Nat. Mater. **11**, 372 (2013).
[3] J.-C. Rojas-Sánchez, N. Reyren, P. Laczkowski, W. Savero, J.-P. Attané, C. Deranlot, M. Jamet, J.-M. George, L. Vila, and H. Jaffrès, Phys. Rev. Lett. **112**, 106602 (2014).
[4] Z. Wei, A. Sharma, A.S. Nunez, P. M. Haney, R. A. Duine, J. Bass, A. H. MacDonald, and M. Tsoi, Phys. Rev. Lett. **98**, 116603 (2007).
[5] H. Nakayama, M. Althammer, Y.-T. Chen, K. Uchida, Y. Kajiwara, D. Kikuchi, T. Ohtani, S. Geprägs, M. Opel, S. Takahashi, R. Gross, G. E. W. Bauer, S. T. B. Goennenwein, and E. Saitoh, Phys. Rev. Lett. **110**, 206601 (2013).
[6] N. Vlietstra, J. Shan, V. Castel, B. J. van Wees, and J. Ben Youssef, Phys. Rev. B **87**, 184421 (2013).
[7] K. Uchida, S. Takahashi, K. Harii, J. Ieda, W. Koshibae, K. Ando, S. Maekawa, and E. Saitoh, Nature (London) **455**, 778 (2008).
[8] K. Uchida, H. Adachi, T. An, T. Ota, M. Toda, B. Hillebrands, S. Maekawa, and E. Saitoh, Nat. Mater. **10**, 737 (2011).
[9] A. Brataas, Physics **6**, 56 (2013).
[10] Y. M. Lu, J. W. Cai, S. Y. Huang, D. Qu, B. F. Miao, and C. L. Chien, Phys. Rev. B **87**, 220409(R) (2013).
[11] Y. M. Lu, Y. Choi, C. M. Ortega, X. M. Cheng, J. W. Cai, S. Y. Huang, L. Sun, and C. L. Chien, Phys. Rev. Lett. **110**, 147207 (2013).
[12] Y. Sun, H. Chang, M. Kabatek, Y.-Y. Song, Z. Wang, M. Jantz, W. Schneider, M. Wu, E. Montoya, B. Kardasz, B. Heinrich, S. G. E. te Velthuis, H. Schultheiss, and A. Hoffmann, Phys. Rev. Lett. **111**, 106601 (2013).
[13] S. Y. Huang, X. Fan, D. Qu, Y. P. Chen, W. G. Wang, J. Wu, T. Y. Chen, J. Q. Xiao, and C. L. Chien, Phys. Rev. Lett. **109**, 107204 (2012).
[14] B. F. Miao, S. Y. Huang, D. Qu, and C. L. Chien, Phys. Rev. Lett. **112**, 236601 (2014).
[15] X. Zhou, L. Ma, Z. Shi, G. Y. Guo, J. Hu, R. Q. Wu, and S. M. Zhou, Appl. Rev. Lett. **105**, 012408 (2014).
[16] B. F. Miao, S. Y. Huang, D. Qu, and C. L. Chien, Phys. Rev. Lett. **111**, 066602 (2013).
[17] G. Y. Guo, Q. Niu, and N. Nagaosa, Phys. Rev. B **89**, 214406 (2014).
[18] T. Kikkawa, K. Uchida, Y. Shiomi, Z. Qiu, D. Hou, D. Tian, H. Nakayama, X.-F. Jin, and E. Saitoh, Phys. Rev. Lett. **110**, 067207 (2013).
[19] M. Schmid, S. Srichandan, D. Meier, T. Kuschel, J.-M. Schmalhorst, M. Vogel, G. Reiss, C. Strunk, and C. H. Back, Phys. Rev. Lett. **111**, 187201 (2013).
[20] D. Qu, S. Y. Huang, J. Hu, R. Q. Wu, and C. L. Chien, Phys. Rev. Lett. **110**, 067206 (2013).
[21] C. Hahn, G. de Loubens, O. Klein, M. Viret, V. V. Naletov, and J. Ben Youssef, Phys. Rev. B **87**, 174417 (2013).
[22] A. H. MacDonald and M. Tsoi, Philos. Trans. R. Soc., A **369**, 3098 (2011).
[23] X. Marti, I. Fina, C. Frontera, J. Liu, P. Wadley, Q. He, R. J. Paull, J. D. Clarkson, J. Kudrnovský, I. Turek, J. Kuneš, D. Yi, J-H. Chu, C. T. Nelson, L. You, E. Arenholz, S. Salahuddin, J. Fontcuberta, T. Jungwirth, and R. Ramesh, Nat. Mater. **13**, 367 (2014).
[24] R. Cheng, J. Xiao, Q. Niu, and A. Brataas, Phys. Rev. Lett. **113**, 057601 (2014).
[25] Y. Y. Wang, C. Song, B. Cui, G. Y. Wang, F. Zeng, and F. Pan, Phys. Rev. Lett. **109**, 137201 (2012).
[26] B. G. Park, J. Wunderlich, X. Martí, V. Hol, Y. Kurosaki, M. Yamada, H. Yamamoto, A. Nishide, J. Hayakawa, H. Takahashi, A. B. Shick, and T. Jungwirth, Nat. Mater. **10**, 347 (2011).
[27] T. Lin, C. Tang, H. M. Alyahayaei, and J. Shi, Phys. Rev. Lett. **113**, 037203 (2014).
[28] H. J. Jiao and G. E. W. Bauer, Phys. Rev. Lett. **110**, 217602 (2013).
[29] Y.-T. Chen, S. Takahashi, H. Nakayama, M. Althammer, S. T. B. Goennenwein, E. Saitoh, and G. E. W. Bauer, Phys. Rev. B **87**, 144411 (2013).
[30] M. Weiler, M. Althammer, M. Schreier, J. Lotze, M. Pernpeintner, S. Meyer, H. Huebl, R. Gross, A. Kamra, J. Xiao, Y.-T. Chen, H. J. Jiao, G. E. W. Bauer, and S. T. B. Goennenwein, Phys. Rev. Lett. **111**, 176601 (2013).
[31] M. Althammer, S. Meyer, H. Nakayama, M. Schreier, S. Altmannshofer, M. Weiler, H. Huebl, S. Geprägs, M. Opel, R. Gross, D. Meier, C. Klewe, T. Kuschel, J.-M. Schmalhorst, G. Reiss, L. Shen, A. Gupta, Y.-T. Chen, G. E. W. Bauer, E. Saitoh *et al.*, Phys. Rev. B **87**, 224401 (2013).
[32] Z. Qiu, K. Ando, K. Uchida, Y. Kajiwara, R. Takahashi, H. Nakayama, T. An, Y. Fujikawa, and E. Saitoh, Appl. Phys. Lett. **103**, 092404 (2013).
[33] P. D. Battle, T. C. Gibb, and C. W. Jones, J. Solid State Chem. **74**, 60 (1988).
[34] I. Fina, X. Marti, D. Yi, J. Liu, J. H. Chu, C. Rayan-Serrao, S. Suresha, A. B. Shick, J. Železný, T. Jungwirth, J. Fontcuberta, and R. Ramesh, Nat. Commun. **5**, 4671 (2014).
[35] A. T. Wong, C. Beekman, H. Guo, W. Siemons, Z. Gai, E. Arenholz, Y. Takamura, and T. Z. Ward, Appl. Phys. Lett. **105**, 052401 (2014).
[36] C. Song, M. Sperl, M. Ulz, M. Ciorga, G. Woltersdorf, D. Schuh, D. Bougeard, C. H. Back, and D. Weiss, Phys. Rev. Lett. **107**, 056601 (2011).